Multiple-quantum dynamics in solid state NMR

J. Baum, M. Munowitz, A. N. Garroway,[a] and A. Pines
Department of Chemistry, University of California, Berkeley and Materials and Molecular Research Division, Lawrence Berkeley Laboratory, Berkeley, California 94720

(Received 17 April 1985; accepted 15 May 1985)

Recently developed solid state multiple-quantum NMR methods are applied to extended coupling networks, where direct dipole–dipole interactions can be used to create coherences of very high order (~ 100). The progressive development of multiple-quantum coherence over time depends upon the formation of multiple-spin correlations, a phenomenon which also accompanies the normal decay to equilibrium of the free induction signal in a solid. Both the time development and the observed distributions of coherence can be approached statistically, with the spin system described by a time-dependent density operator whose elements are completely uncorrelated at sufficiently long times. With this point of view, we treat the distribution of coherence in a multiple-quantum spectrum as Gaussian, and characterize a spectrum obtained for a given preparation time by its variance. The variance of the distribution is associated roughly with the number of coupled spins effectively interacting, and its steady growth with time reflects the continual expansion of the system under the action of the dipolar interactions. The increase in effective system "size" is calculated for a random walk model for the time development of the density operator. Experimental results are presented for hexamethylbenzene, adamantane, and squaric acid. The formation of coherence in systems containing physically isolated clusters is also investigated, and a simple method for estimating the number of spins involved is demonstrated.

I. INTRODUCTION

Most applications of ^{1}H multiple-quantum NMR spectroscopy have necessarily been limited to small spin systems in isotropic or partially oriented phases, where the size of the system is clearly defined by the nature and extent of the spin–spin coupling.[1,2] In liquids, for example, only indirect scalar coupling remains after anisotropic interactions have been averaged to zero by rapid isotropic molecular motion. If, instead, the molecules are dissolved in a nematic liquid crystal, translational freedom is retained but reorientation via tumbling is restricted so that intramolecular dipolar coupling becomes the principal interaction among the spins. In either case the spin–spin interactions are short range, and the system usually remains small enough to be characterized by a density operator that can be constructed from a finite, manageable number of basis operators.[3] In this regard, expansions based on fictitious spin-1/2,[4] spherical tensor,[5] and product[6] operators have proved quite useful for describing many experiments involving multiple-quantum effects. Among the numerous applications reported to date have been methods to simplify complicated single-quantum spectra,[7] determine spin connectivity and topology,[8] obtain high-resolution spectra in inhomogeneous magnetic fields,[9] and facilitate coherence transfer and indirect detection in systems containing magnetically rare nuclei.[10] On the other hand, the extension of ^{1}H multiple-quantum spectroscopy to strongly coupled *solids*, where the coupling network includes all the spins in the sample, has also been illustrated recently.[11] This work has demonstrated that high order multiple-quantum coherences can be prepared and detected in solids, provided that time reversal excitation is used to counter the effects of dipolar dephasing.[12]

Our interest here is to follow the development of multiple-quantum coherence in a solid, visualizing experimentally the emergence with time of a widening network of multiple-spin correlations throughout the system. This phenomenon provides some insight into the decay of the single-quantum free induction signal in a solid, and also leads us to the notion of an instantaneous effective size for the system, which increases monotonically until it approaches a macroscopic number of spins. In this paper we use multiple-quantum methods to study these aspects of nuclear spin dynamics in protonated solids. The preparation and detection of multiple-quantum coherence is illustrated for a variety of systems, and the concept of a time-dependent, effective spin size is then quantified within the framework of a statistical model. Time-resolved measurements of the effective number of spins interacting in a solid are used further to probe the nature of the dipolar coupling among the spins. Specifically, information about the relative magnitudes of intermolecular and intramolecular dipolar interactions and about the existence and sizes of local clusters of spins can be obtained from a careful analysis of the solid state multiple-quantum spectra.

II. THEORY

A. Spin interactions in a rigid lattice

A collection of N interacting spin-1/2 nuclei in a magnetic field can be described by an internal Hamiltonian,

$$H_{\rm int} = H_z + H_{zz}, \tag{1}$$

consisting of a chemical shift (or resonance offset) term

$$H_z = -\sum_{i=1}^{N} \Delta\omega_i I_z \tag{2}$$

[a] Permanent address: Code 6120, Naval Research Laboratory, Washington, D. C. 20375.

 0021-9606/85/172015-11$02.10

and a dipolar coupling term

$$H_{zz} = -\sum_{i<j} D_{ij}(3I_{zi}I_{zj} - \mathbf{I}_i\cdot\mathbf{I}_j) \tag{3}$$

that is bilinear in the spin angular momentum operator. Each coupling constant (D_{ij}) is inversely proportional to the cube of the distance between spins i and j, and is measured in units of angular frequency. The internal Hamiltonian commutes with the external, or Zeeman, Hamiltonian, so that each eigenstate $|i\rangle$ of $H_{\rm int}$ is characterized by a magnetic quantum number M_i and an internal eigenfrequency ω_i. The complexity of the system precludes an exact, analytical calculation of the eigenstates and eigenvalues; nevertheless, it can be asserted that the eigenvalues do exist and that their spectrum of frequencies is quasicontinuous for large N.[13]

The system, described by its density operator ρ in the rotating frame, evolves under $H_{\rm int}$ according to the quantum-mechanical Liouville equation,

$$\rho(t) = \exp(-iH_{\rm int}\,t)\,\rho(0)\exp(iH_{\rm int}\,t), \tag{4}$$

which, in the $|i\rangle\langle j|$ operator basis, becomes

$$\rho(t) = \sum_{ij}\langle i|\rho(0)|j\rangle\exp[-i(\omega_i-\omega_j)t\,]\,|i\rangle\langle j|. \tag{5}$$

Knowledge of the density operator at any time permits the calculation of any desired property of the spin system.

B. Multiple-spin processes and the free induction decay

Our approach to the study of spin dynamics in large systems employs multiple-quantum NMR to monitor concerted interactions in groups of spins. Multiple-quantum coherences, described in the $|i\rangle\langle j|$ representation by off-diagonal elements of $\rho(\tau)$ for which $n = M_i - M_j \neq \pm 1$, can be excited using pulse methods and detected indirectly in a two-dimensional experiment.[14]

The basic division of a multiple-quantum experiment into distinct preparation (τ), evolution (t_1), mixing (τ'), and detection (t_2) periods is illustrated in Fig. 1, and several specific pulse sequences are shown in Fig. 2. A simple and widely known example, composed of three ($\pi/2$) pulses,[14] is depicted in Fig. 2(a). Although this particular version is not designed for solids, we can use it here to grasp the essential features of the problem before specializing to the more sophisticated sequences described in the next section. The important point to note is that the eventual multiple-quantum spectrum is determined by the distribution of multiple-spin operators at the end of the preparation period, which in this case is marked by the second pulse. However, just prior to the application of the second pulse, the system has simply undergone free evolution following a single ($\pi/2$) pulse. Consequently, the growth of multiple-quantum coherence and the decay of the free induction are necessarily linked, since both phenomena depend upon the development of similar many-body correlations among the coupled spins.

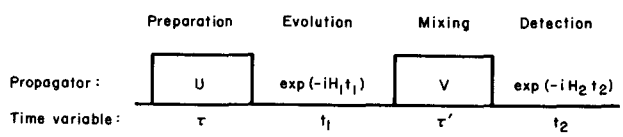

FIG. 1. General form of the multiple-quantum pulse sequence. Multiple-quantum coherences are created by the preparation period propagator $U(\tau)$ and respond to local fields during the evolution period t_1. The mixing period propagator $V(\tau)$ transfers multiple-quantum coherence to single-quantum coherence for detection during t_2.

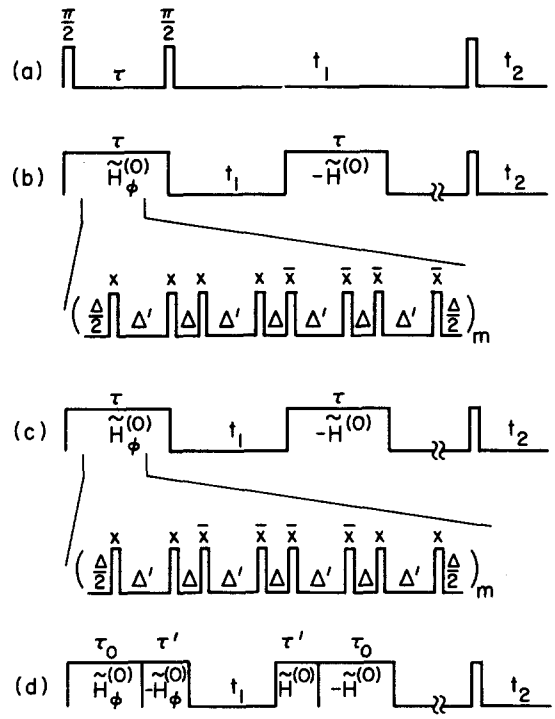

FIG. 2. Pulse sequences for multiple-quantum NMR: (a) Basic three-pulse experiment suitable for systems where individual transitions can be resolved. (b) and (c) Time reversal sequences used for solids. The preparation and mixing propagators, generated by m cycles of eight $\pi/2$ pulses with duration t_p and spacings of Δ and $\Delta' = 2\Delta + t_p$, produce $\tilde{H}^{(0)} = \frac{1}{3}(H_{yy} - H_{xx})$ for RF phases x and $\bar{x}$ and $\tilde{H}^{(0)} = -\frac{1}{3}(H_{yy} - H_{xx})$ for RF phases y and $\bar{y}$. To separate the multiple-quantum orders, the relative phase ϕ between preparation and mixing is incremented in proportion to the evolution time t_1. About 2 ms after mixing, the z component of magnetization is monitored with the aid of an x pulse followed by a 100 μs spin locking pulse (symbolized here by a single pulse). One point is sampled for each value of t_1, and the time-domain data are Fourier transformed with respect to t_1 to produce the multiple-quantum spectra. (d) Experiment designe to refocus multiple-quantum coherence in solids. High-order coherences created during τ_0 evolve backwards in time during τ' to return to low-order coherences. (See Sec. IV B.)

To be more explicit, we consider first the origins of dipolar dephasing in a rigid lattice. For the initial condition

$$\rho(0) = I_x = \sum_{i=1}^{N} I_{xi}, \tag{6}$$

which is obtained when the system in thermal equilibrium is subjected to the first $\pi/2$ pulse, the observable magnetization is given by

$$S_x(\tau) = \mathrm{Tr}[\,\rho(\tau)I_x\,] = \sum_{i<j}|\langle i|I_x|j\rangle|^2\exp[i(\omega_i-\omega_j)\tau]. \tag{7}$$

This expression shows that the spectrum of allowed frequencies is limited to those connecting pairs of states $|i\rangle$ and $|j\rangle$ which differ by $n = \pm 1$. The single quantum signal decays with time, owing simply to destructive interference among

the numerous modes of oscillation.[13]

Having noted this point, we can express the density operator in a basis which clearly illustrates the essential features involved both in the loss of observable magnetization with time, and with the appearance of correlations among increasing numbers of spins: The density operator $\rho(\tau)$ [Eq. (4)] naturally takes on a product form when written as a power series; viz.

$$\rho(\tau) = \rho(0) + i\tau[\,\rho(0), H_{\rm int}\,] - \tfrac{1}{2}\tau^2[\,[\,\rho(0), H_{\rm int}\,], H_{\rm int}\,] + \cdots . \quad (8)$$

Substitution of Eqs. (1)–(3) and (6) into Eq. (8) reveals the basic features of free evolution under the dipolar Hamiltonian. The nested commutators produce product terms, such as $I_{zq}\, I_{zq-1}\cdots I_{z2}\, I_{x1}$, which involve q interacting spins and which are associated with powers of $D_{ij}\,\tau$. A conventional NMR experiment is sensitive to the values of the coefficients associated with I_x and I_y single-spin operators. Under free evolution in the presence of a bilinear Hamiltonian, the density operator acquires additional product terms which are invisible to the detector, and the observable magnetization diminishes. The loss of magnetization in a system of rigidly held spins is not irreversible, however, since the norm of ρ is conserved under the unitary transformation of Eq. (4). Rather, the new terms, which reflect the development of complex correlations among increasing number of spins, increase their amplitudes at the expense of the observable terms.

C. Time development of the dipolar coupling network

The influence of a coupling between two spins on the development of the system depends on the time elapsed, with the value of $D_{ij}\,\tau$ providing a measure of the effectiveness of a particular pair interaction at each instant. When $D_{ij}\,\tau \ll 1$, insufficient time has elapsed for the interaction between i and j to be significant. However, as time passes, more couplings become sufficiently large to contribute beyond first order, and the number of admissible single-spin operators increases. The contribution of these high-order terms to the power series becomes more and more important with time. In addition, the strongly coupled spins which determine the early time development continue to influence the dynamics at later times. Overall, long periods of free evolution allow more spins to communicate fully with each other via their dipolar coupling and the effective "size" of the system grows. To emphasize this point, we show in Fig. 3 a symbolic representation of the growth of multiple-spin correlations under a many-body bilinear Hamiltonian. When the system has evolved to the point where many spins are able to act in concert, application of the second pulse can transform a term like $I_{zq}\cdots I_{z2}\, I_{x1}$, which represents single quantum coherence of spin $k=1$, into terms representing coherences between all possible combinations of all q spins. The simplest example, the presence of double-quantum and zero-quantum coherence between spins k and l, arises from a term such as $I_{kx}\, I_{lx}$, which connects states differing by $n=2$ and $n=0$. In the general case, coherences among any number of spins, up to the effective size of the system at time τ, can be created.

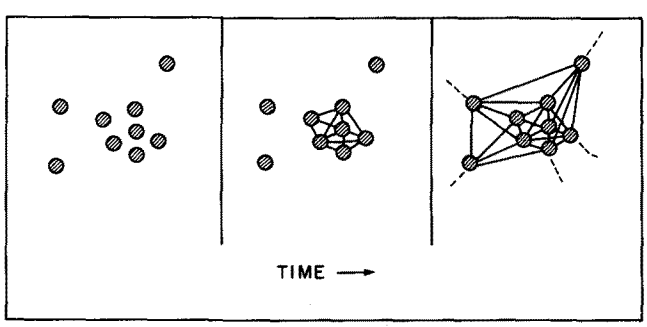

FIG. 3. Symbolic representation of the growth of a coupling network with time. Initially, the spins act independently, having had insufficient time to communicate via dipole–dipole interactions. Pairwise couplings become effective as time passes. Roughly speaking, small dipole–dipole couplings require longer "propagation times" than large ones.

D. Approach to multiple-quantum NMR in solids

Where an extensive network of dipolar couplings exist, as in a typical protonated solid, coherences of very high order are possible. However, if multiple-quantum signals are to be observed, certain steps must be taken to insure that all contributions to a given order of coherence are generated with the same phase. Otherwise, destructive interference among the innumerable lines within an order will severely attenuate the signal.[11]

The intensity and phase of an individual multiple-quantum line are determined by the detailed history of the spin system up to the point of detection. In the general case, where propagators $U(\tau) = \exp(-iH\tau)$ and $V(\tau') = \exp\times(-iH'\tau')$ govern the dynamics during the preparation and mixing periods, the detectable magnetization at $t_2 = 0$ is given by

$$\begin{aligned} S(\tau,t_1,\tau') &= \mathrm{Tr}\, I_z\, \rho(\tau,t_1,\tau') \\ &= \mathrm{Tr}\, I_z\, V^\dagger(\tau')\exp(-iH_{\rm int}t_1)U^\dagger(\tau) I_z\, U(\tau) \\ &\quad \times \exp(iH_{\rm int}t_1)V(\tau'). \end{aligned} \quad (9)$$

Defining complex matrix elements $P_{ij} = \langle i|U^\dagger I_z U|j\rangle$ and $Q_{ji} = \langle j|V I_z V^\dagger|i\rangle$, we can express this signal as

$$S(\tau,t_1,\tau') = \sum_{i,j} P_{ij}(\tau)Q_{ji}(\tau')\exp[-i(\omega_i-\omega_j)t_1], \quad (10)$$

from which it is clear that the phase factor associated with each transition may be different for every oscillation frequency. However, if the propagator V can be made either equal to $U^\dagger$ or different from it only by a phase factor χ, then

$$V = \exp(-i\chi I_z)U^\dagger \exp(i\chi I_z), \quad (11)$$

and the signal reduces to a Fourier series with real coefficients:

$$S(\tau,t_1,\tau') = \sum_n \sum_{i,j} |P_{ij}|^2 \exp(in\chi)\exp[-i(\omega_i-\omega_j)t_1]. \quad (12)$$

Now all lines within a given order have the same phase, and lines between neighboring orders differ in phase by $\pm\chi$.

The requirement that V and U be Hermitian conjugates can be satisfied if the preparation and mixing Hamiltonians

are equal in magnitude but opposite in sign. This condition, which results from an apparent time reversal,[12] is brought about using coherent averaging methods, as shown in Ref. 11. The result is that very high-order coherences can be observed in solids, without loss of signal from phase cancellation.

III. EXPERIMENTAL CONSIDERATIONS

A. Pulse sequence design

1. Preparation period

Coherences of even order can be created with a nonsecular even-quantum average Hamiltonian, such as

$$\tilde{H}(0) = \tfrac{1}{3}(H_{yy} - H_{xx})$$

$$= -\tfrac{1}{2}\sum_{i<j} D_{ij}(I_{i+}\, I_{j+} - I_{i-}\, I_{j-}), \tag{13}$$

where $I_{j\pm} = I_{jx} \pm iI_{jy}$.[7(b)] This desired average Hamiltonian is attainable with a variety of specific pulse trains, each employing a four-pulse subcycle as the basic design unit. In the limit of infinite RF power, any series of x and $\bar{x}$ pulses with alternating delays of Δ and 2Δ will produce the average dipolar Hamiltonian $\frac{1}{3}(H_{yy} - H_{xx})$, provided that the interaction is cyclic. The overall sequence can be compensated for RF inhomogeneity and resonance offset effects by the proper combination of two or more subcycles.

Two different eight-pulse cycles used in the experiments to be reported are shown in Figs. 2(b) and 2(c). Both pulse sequences consist of $\pi/2$ pulses of duration t_p, separated by delays Δ and $\Delta' = 2\Delta + t_p$. The finite width of the pulses is accounted for in the long delay, Δ', and the cycle time, t_c, is equal to $12(t_p + \Delta)$ in each case. Sequence 2(b) is preferred whenever resistance to resonance offset effects during preparation and mixing is particularly important. For example, in multiple-quantum *imaging* experiments in solids,[15] coherences must be prepared in the presence of large offsets created by the imposition of an external field gradient. By contrast, sequence 2(c) is more appropriate in cases when rf inhomogeneity is a serious problem.

Although the density operator prepared at time τ contains predominantly even-order coherences, pulse imperfections can lead to the creation of unwanted odd-order coherences. These can be reduced by cycling the phases of all pulses in the preparation period between 0° and 180° in alternate experiments, and coadding the resulting signals appropriately.[16] In addition, it is necessary to label the orders of coherence by the overall RF phase of the preparation period. The method of time proportional phase incrementation (TPPI),[5,17] under which the phases of the preparation pulses are augmented regularly for each value of t_1, serves to introduce an artificial offset term into the *evolution* period. Fourier transformation of the resulting multiple-quantum interferogram then separates orders $n = M_i - M_j$ in the frequency domain, as suggested by Eq. (12) for $\Delta\chi = \Delta\omega\Delta t_1$.

2. Evolution period

During the evolution period, the system responds to the internal Hamiltonian,

$$H_{\text{int}} = H_z + H_{zz}, \tag{1}$$

where H_z formally contains an order-dependent offset term resulting from TPPI. The interferogram is mapped out point-by-point for successive values of t_1. The spectral width of the multiple-quantum spectrum is given by $1/\Delta t_1$, and the number of orders detected, $\pm n_{\max}$, is determined by the phase increment, $\Delta\phi = 2\pi/2n_{\max}$. Both Δt_1 and $\Delta\phi$ must be chosen so that all signals from different coherence orders fit into the available bandwidth without aliasing and without overlapping.

3. Mixing period

After evolving in the local fields for a time t_1, the multiple-quantum coherences are converted to observable single-quantum coherences through the action of the mixing period propagator $V(\tau)$. Since the average Hamiltonian of Eq. (13) is a pure double-quantum operator, time reversal is accomplished here by a simple 90° phase shift of each pulse in the eight-pulse cycle. The mixing period therefore contains pulses with phases y and $\bar{y}$, irrespective of any manipulations of the phases in the preparation period.

4. Detection period

After mixing, a 2 ms delay is inserted, during which spurious transverse magnetization is allowed to decay. The desired signal, stored as population information along the z axis, is detected with a $(\pi/2)_x$ pulse, followed by a 100 μs spin-locking pulse along y. Spin temperature inversion,[18] achieved by a 180° phase alternation of the detection pulse, is used to reduce artifacts arising from receiver ringing. A single point in t_2 is then sampled for each value of t_1, with the width of the single-quantum spectrum determining the optimum receiver bandwidth.

B. Implementation

Experiments were performed on two home-built spectrometers operating at ^{1}H Larmor frequencies of 360 and 180 MHz.[19,20] Both spectrometers are equipped with quadrature phase generation circuits that produce RF pulses with relative phases of 0°, 90°, 180°, and 270° at 30 MHz IF. Additional phase shifts needed for TPPI are generated by a 30 MHz 8-bit digital phase shifter in series with the quadrature generation network.

Pulse widths and phases must be set carefully with the aid of a standard (H_2O) tune-up sequence before each experiment.[21,22] The overall performance of the matched preparation/mixing periods is optimized by adjusting the total RF amplitude to obtain maximum signal for $t_1 = 0$, $\Delta t_1 = 0$. With the preparation and mixing sequences arranged "back-to-back", the experiment is reduced to a simple time reversal procedure. The optimum cycle time is then selected by varying t_c to peak the signal obtained at a fixed value of τ. Signal losses occur because the time reversal sequence begins to fail at long τ. Pulse imperfections and effects due to higher-order correction terms accumulate over many cycles, and the subsequent degradation in performance ultimately reduces the S/N in the multiple-quantum spectra.

The pulse programmer for each spectrometer is gov-

erned by a 10 MHz clock, which limits the minimum increment in t_1 to 100 ns. When additional bandwidth is needed to accommodate the multiple-quantum spectrum, we use a home-built delayed clock generator to shift the phase of the clock pulses by one, two, or three quarter cycles. Increments of 25, 50, 75 ns thus become available, increasing the bandwidth to 40 MHz. Ultimately, the performance of the experiment is limited by the accuracy of the phase shifter: A small phase error $\delta\phi$ will introduce a phase shift of $n\delta\phi$ for each order, and will inevitably become a big phase error when n becomes sufficiently large.[23]

C. Samples

Before presenting experimental results, we note some basic room temperature structural and dynamical properties of the molecular systems to be studied. The molecules are diagrammed in Fig. 4.

1. Adamantane ($C_{10}H_{16}$; polycrystalline)

Adamantane forms a plastic crystal in which the nearly spherical molecules tumble rapidly and isotropically in the solid phase. The motion averages all intramolecular dipolar couplings to zero, but does not eliminate intermolecular couplings. However, the motion leaves only one distinct coupling between every pair of molecules, thereby reducing the adamantane molecule to a point dipole source containing 16 spins. The molecules pack into a face-centered-cubic lattice, with each adamantane molecule surrounded by 12 neighbors at a distance of 6.60 Å, 6 more at 9.34 Å, and an additional 16 at 11.4 Å.[24]

2. Hexamethylbenzene [$C_6(CH_3)_6$; polycrystalline]

Hexamethylbenzene (HMB) exists in a triclinic unit cell with the planar benzene rings forming a nearly hexagonal net.[25] Two varieties of anisotropic molecular motion determine the dipolar properties of this system. First, each methyl group rapidly reorients about its C_3 axis, rendering the three ^{1}H nuclei equivalent. Second, the entire molecule undergoes fast-limit sixfold hopping about the C_6 axis of the benzene ring,[26] which reduces the intramolecular dipolar couplings between *ortho*, *meta*, and *para* methyls. Intermolecular couplings remain but, as in adamantane, interacting molecules behave as point sources. Within a molecule, average distances between protons on different methyl groups range from 3.3 Å (*ortho*) to 6.6 Å (*para*), and between molecules, C–C distances range upwards from 3.7 Å. Sheets of molecules in the *a–b* plane are separated by 5.3 Å.

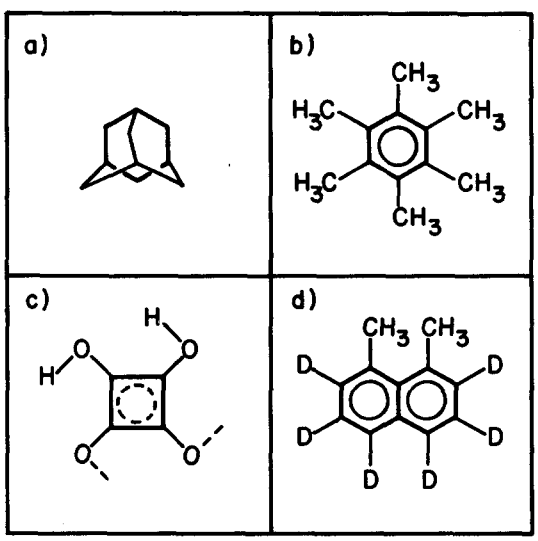

FIG. 4. Systems studied: (a) Adamantane, (b) hexamethylbenzene, (c) squaric acid, (d) 1,8- dimethylnaphthalene-d_6.

3. Squaric acid ($C_4O_4H_2$; single crystal)

Squaric acid is monoclinic but pseudo-body-centered tetragonal at room temperature. It is a layered two-dimensional structure consisting of hydrogen-bonded "squaric" subunits of C_4O_4. The hydrogens form chains perpendicular to the *a–c* plane, with the hydrogens in different sheets separated by $b/2 = 2.6$ Å.[27] During the experiment the crystal was oriented with the *b* axis perpendicular to the static magnetic field. The crystal was doped with chromium ions to reduce the ^{1}H spin-lattice relaxation time.

4. Partially deuterated 1,8-dimethylnaphthalene ($C_{12}H_6D_6$; polycrystalline)

1,8-dimethylnaphthalene (DMN) forms a monoclinic structure, with the methyl hydrogens on adjacent molecules facing each other in pairs. The shortest intermolecular ^{1}H–^{1}H contact is approximately 2.0 Å along the *b* axis, and the intramolecular methyl substituents are separated by 2.93 Å.[28] All positions on the rings have been deuterated in order to isolate the 12 methyl protons in the dimeric units.

IV. RESULTS AND DISCUSSION

A. Multiple-quantum excitation dynamics

1. Effective cluster size

Figure 5 contains a set of ^{1}H multiple-quantum spectra obtained from hexamethylbenzene using sequence 2(b) with preparation times ranging from 66 to 792 μs. These plots illustrate the distribution of spectral intensity over the coherence orders at the specified preparation times. Separation of the different orders has been accomplished by TPPI, so that the subspectrum of each order n occupies 156.25 kHz. Since coherences of $+n$ and $-n$ are equally probable, the full spectra are naturally symmetric about $n = 0$. Consequently, only one-half of each spectrum is needed to obtain all the information available.

A general tendency for coherences of higher order to develop with time is clearly evident in the spectra shown in Fig. 5; the results are particularly striking for $\tau = 792$ μs, where there are strong signals extending out to, and apparently beyond, $n = 64$. The experimentally observed redistribution of spectral intensity into high-order coherences is a tangible manifestation of the growth of multiple-spin correlations during the preparation period. Subspectral structure and linewidths are determined by the response of the prepared system to the local field of all the other spins during

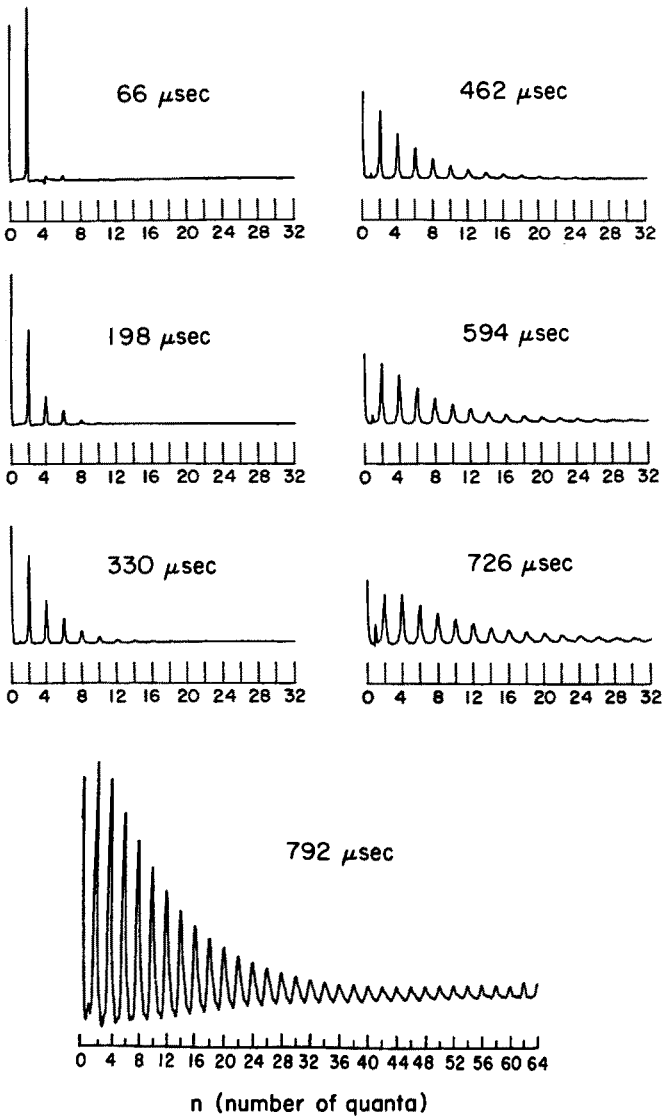

FIG. 5. 360 MHz ^{1}H multiple-quantum spectra of hexamethylbenzene for $\tau = 66$ to $\tau = 792$ μs recorded with sequence (b) of Fig. 2. The basic cycle time in these experiments, and in all others to be reported here, is 66 μs ($t_p = 3\,\mu$s, $\Delta = 2.5\,\mu$s, and $\Delta' = 8\,\mu$s). For $\tau = 66$ to 462 μs, the t_1 increment is 100 ns and the phase increment is $2\pi/64$; this separates each order by 156.25 kHz. For $\tau > 528$ μs, the t_1 and phase increments are 50 ns and $2\pi/128$, respectively. The distribution of spectral intensity over the coherence orders broadens continuously as the preparation time increases. The lowermost trace, an expanded view of the spectrum obtained for $\tau = 792$ μs, emphasizes the highest orders of coherence observed.

the subsequent evolution period. Here, a spectrum of broad featureless lines arises from the almost continuous distribution of eigenfrequencies in a sample containing virtually an infinite number of spins.

Exact calculation of the time development of a large and complex spin system is usually impossible, owing both to the limits of computing power and to the need for prior knowledge of an enormous number of spin–spin couplings. However, for very short preparation times,

$$\rho(\tau) \approx \rho(0) + i\tau[\,\rho(0), H_{\rm int}\,] - \tfrac{1}{2}\tau^2\,[\,[\,\rho(0), H_{\rm int}\,], H_{\rm int}\,] \qquad (14)$$

so the excitation dynamics are initially determined only by the very strongest dipolar couplings. If, for simplicity, we assume that at later times the infinite spin system can be partitioned into *finite* spin systems, and, further, that all possible coherences have been excited with equal probability, then calculation of the growth of the distribution of coherence is reduced to a combinatorial problem. The total intensity within a given order is related simply to the number of different ways of arranging the states consistent with the value of n.[29] However, in making this assumption, we are attempting to extend a concept familiar from systems where the number of coupled spins is well defined. For the case of small molecules oriented in liquid crystal solvents, earlier experimental and theoretical studies have validated the assumption of equal coherence magnitudes after long periods of excitation.[30] However, the situation in a dipolar solid is considerably more complex since the number of interacting spins is never really well defined. For example, while coherence within some finite cluster of spins may have been excited to a limiting value after a given time, higher-order coherence arising from a larger cluster may still be present, although less developed.

We address this question in Fig. 6, where we examine the time development of the 4-, 8-, 12-, and 16-quantum transitions in HMB by plotting the integrated intensity of each line, normalized to the total spectral intensity, vs preparation time. The graph suggests that contributions from different orders of coherence peak at well separated intervals, so that at any specified preparation time, clusters exceeding some nominal range of sizes hardly affect the dynamics at all. Consequently, we can, with some justification, account for a very complicated time development by characterizing the system by a single time-dependent cluster size, $N(\tau)$.

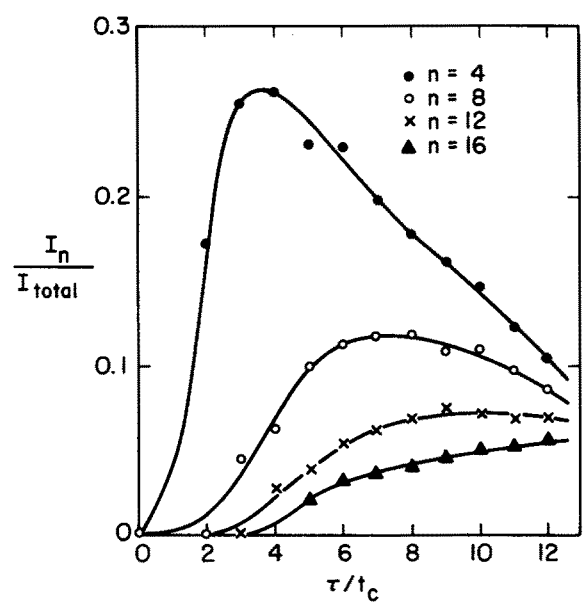

FIG. 6. Intensity vs preparation time for $n = 4$, 8, 12, and 16 in HMB. The intensity for each order has been normalized relative to the total spectral intensity, and smooth curves have been drawn through the data points to aid the eye. Contributions from different orders of coherence grow in at different rates, consistent with the notion that a finite number of spins can be used to characterize the system at any time.

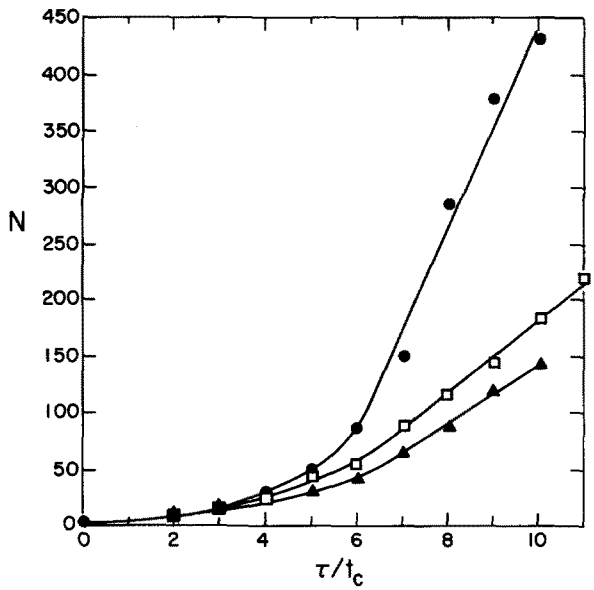

FIG. 7. N vs τ/t_c for adamantane (circles), hexamethylbenzene (squares), and squaric acid (triangles). The smooth curves through the points emphasize the continuous expansion of the effective size of the unbounded spin systems.

Among this group of N interacting spin-1/2 nuclei, the number of equivalent configurations for a coherence of nonzero order is $(2N)!/[(N-n)!(N+n)!]$, which is well approximated by $2^{2N}(N\pi)^{-1/2}\exp(-n^2/N)$ for $N>6$. In this picture a multiple-quantum intensity distribution can be described by a Gaussian curve with variance $\sigma^2 = N(\tau)/2$. The variance of the distribution is thus associated roughly with the number of spins among which coupling has been established within the time limit of the preparation period. However, since such a frontier is normally indistinct in a solid, $N(\tau)$ is best regarded as a parameter of a particular system. Its change with time is determined by the structure of the solid, and is influenced by factors such as spin topology and the relative magnitudes of intramolecular and intermolecular dipolar interactions. Ultimately, all the spins become correlated in a network of macroscopic size.

Values of $N(\tau)$ vs τ for hexamethylbenzene, adamantane, and squaric acid, are plotted in Fig. 7. These were obtained by fitting the integrated intensities of the lower orders to a Gaussian distribution. The intensity of each order was normalized relative to $n=2$ for each preparation time. In this manner reasonable estimates for N can be obtained even when the very highest orders possible cannot be observed experimentally. Deviations from strictly statistical behavior are most pronounced in the tail of the distribution, where the combinatorial method consistently underestimates the intensities of the highest orders.[30]

2. Random-walk model

Many statistical interpretations of the multiple-quantum excitation dynamics are possible. Here we model the increase of $N(\tau)$ with τ by adopting a purely stochastic view of the *time development* of $\rho(\tau)$ for long τ. In this limit, reached perhaps after three or four dipolar correlation times, the values of matrix elements $\rho_{ij}(\tau)$ at different times are least likely to appear correlated, and a simple time dependence may become apparent.

In general, the density operator for N spins can be represented compactly by an expansion in product operators,

$$\rho(\tau) = \sum_s b_s(\tau)\, B_s(q,N) \tag{15}$$

with the 2^{2N} basis operators,

$$B_s(q,N) = 2^{(q-1)} \prod_{k=1}^{N} (I_{kv})^{a_k} \tag{16}$$

forming a complete orthonormal set, defined by $\mathrm{Tr}(B_s B_t) = \delta_{st}$.[6] In the expression above, $v = x, y$, or z, and q is the total number of single-spin operators in the product. The exponent a_k takes on the value 1 for the q operators of interest and 0 for the remainder. In the picture of multiple-quantum excitation dynamics described above, the effective spin size, $N(\tau)$, is allowed to expand with increasing preparation times. Consequently, the space basis operators needed to represent $\rho(\tau)$ expands as well. If, in the statistical limit, elements of the density operator at different times are truly uncorrelated, then the time development of the system can be treated as a random walk over the space of product operators which represents all possible multiple-spin states. The probability that an operator $B(q,N)$ at τ will "jump" to an operator $B(q',N')$ at τ' is then simply the product of the degeneracies of the two operator manifolds. The basic assumption is that all elements of ρ are equally accessible under the multiple-quantum Hamiltonian, which, given the complexity of the dynamics and the long times involved, is not unreasonable.

A random walk over product operator space is illustrated schematically in Fig. 8. In this picture, one set of terms,

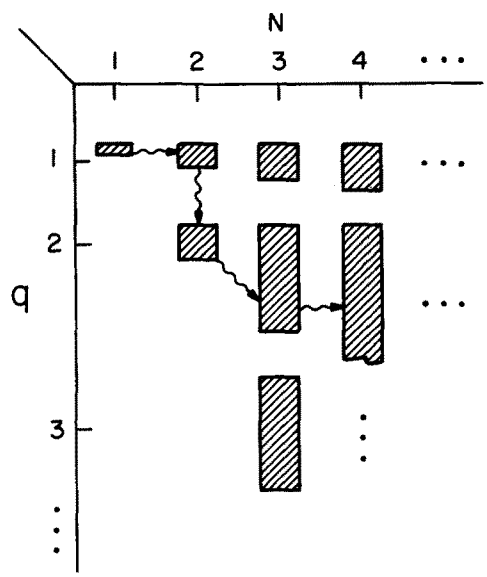

FIG. 8. Schematic representation of a random walk over a space of product operators used to form a basis for the density operator. The space consists of $2^{2N}-1$ linearly independent q-spin operators ($1 \leq q \leq N$), excluding the unit operator. The sizes of the blocks have been chosen to illustrate the relative proportions of q-spin operators in a manifold of N spins. The dimensionality of the space is allowed to expand to stimulate the growth of the effective size of the spin system.

the q-spin operators $B(q,N)$, is monitored as it moves throughout the expanding operator space. Nine options are provided for $B(q,N)$ to jump to $B(q',N')$, i.e.,

$$\begin{cases} q-2, & N-1 \\ q, & N-1 \\ q+2, & N-1 \end{cases}$$
$$(q,N) \rightarrow \begin{cases} q-2, & N \\ q, & N \\ q+2, & N \end{cases}$$
$$\begin{cases} q-2, & N+1 \\ q, & N+1 \\ q+2, & N+1 \end{cases}$$

provided that $0 < q' \leqslant N'$. These pathways have been selected to approximate the operators actually accessible under the even-quantum Hamiltonian of Eq. (13). The number of q-spin operators $B(q,N)$ at any step is given by

$$\zeta_{qN} = \frac{N!}{q!(N-q)!} 3^q, \tag{17}$$

so the normalized probability for the move $B(q,N) \rightarrow B(q',N')$ is simply

$$P_{qNq'N'} = \frac{\zeta_{qN}\zeta_{q'N'}}{\sum_{q'N'} \zeta_{qN}\zeta_{q'N'}}. \tag{18}$$

The trajectory is determined by comparing the statistical probabilities at each step to a random number, as in a Monte Carlo approach. The time development of N is thus directly available, and can be compared to the time dependence observed in the experimental spectra.

A typical simulation is shown in Fig. 9. This plot of N vs number of steps clearly indicates a linear dependence in the statistical limit. On average, the effective size of the system increases by 1 in approximately 73% of the moves, is unchanged in approximately 21% of the moves, and decreases by 1 for the remaining 6%. These probabilities provide an overwhelming impetus for the system size to grow, apparently monotonically, with time. Although other pathways can be selected in a model of this type, the basic time dependence remains unchanged. The data plotted in Fig. 7 suggest that the onset of statistical behavior occurs after $\sim 300\,\mu$s for the systems studied.

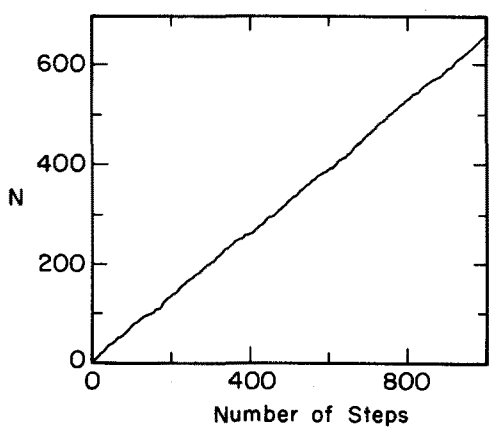

FIG. 9. Monte Carlo simulation of a random walk over product operator space, with $\Delta N = 0, \pm 1$ and $\Delta q = 0, \pm 2$. The curve is the result of averaging 100 independent trials of 1000 steps.

B. Monitoring of time reversal via the refocusing of multiple-quantum coherence

It is perhaps not surprising that the excitation of multiple-quantum coherence in a dipolar solid can be approached as a random walk problem, in view of the connection between multiple-quantum events and some other more well known consequences of evolution under a bilinear Hamiltonian. For example, spin diffusion, an intuitively appealing concept originally introduced by Bloembergen[31] to explain unexpectedly short T_1's in CaF_2, also shares many of the qualitative features of macroscopic, random diffusion. Nevertheless, the apparent success of diffusive models of nuclear spin dynamics belies an underlying regularity demanded by the quantum mechanical equations of motion. Although it may appear to be stochastic, the time development of a spin system according to Eq. (4) is actually well determined, and can be reversed if the sign of the effective internal Hamiltonian is changed.

That coherent averaging methods can reverse supposedly irreversible dipolar dephasing has already been amply demonstrated by "magic echo" experiments.[12] However, we can gain added insight into such dephasing and rephasing by visualizing the time reversal process explicitly through multiple-quantum spectroscopy. The novelty here is that we can show how time reversal is effective even for very high-order, multiple-spin processes.

Sequence (d) of Fig. 2 is designed to reverse the formation of the network of spin correlations common to both multiple-quantum excitation and spin "diffusion." The plan is to allow couplings to develop normally for a rather long, fixed time τ_0, and then to focus the multiple-quantum coherences over the interval τ'. The refocusing during τ' is accomplished by phase shifting the excitation pulses by 90° to change the sign of the average Hamiltonian. The mixing period is altered symmetrically to fulfill the requirement for overall time reversal relative to the preparation period.

The reversibility of multiple-quantum excitation is illustrated experimentally in Fig. 10. Shown at the left are three 180 MHz ^{1}H spectra of adamantane obtained in the usual fashion with sequence 2(c) and $\tau = 462$, 330, and 66 μs. Directly opposite are the equivalent refocused spectra, recorded with $\tau_0 = 528\,\mu$s and $\tau' = 66$, 198, and 462 μs. In each case, the net forward preparation times are identical, since $\tau = \tau_0 - \tau'$. To the extent that the time reversal works perfectly, the development of *all* the multiple-quantum coherences during τ_0 will be retraced during the τ' interval, during which the clock governing the dipolar Hamiltonian appears to run backwards. Indeed, the spectra to be compared in Fig. 10 are reasonably similar. In particular, note that for $\tau = 66$ μs, only two-quantum coherence is observed after normal excitation by sequence 2(c). For the comparable spectrum produced by sequence 2(d) the system generates coherences up to $n = 32$ during the initial development period of 528 μs, and then reverses the process for $\tau' = 462\,\mu$s to leave primarily two-quantum coherence.

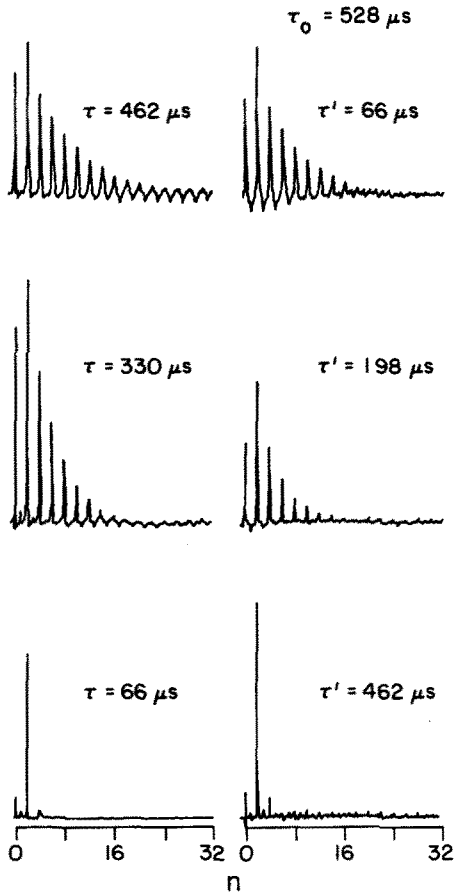

FIG. 10. 180 MHz ^{1}H spectra of adamantane illustrating the feasibility of refocusing multiple-quantum coherence via time reversal. Phase cycling and spin temperature inversion have not been implemented in this experiment. Left: Spectra obtained with sequence (c) of Fig. 2 for $\tau = 66$, 330, and 462 μs. High-order coherences develop normally with $\tilde{H}^{(0)} = \frac{1}{3}(H_{yy} - H_{xx})$ during the preparation period. Right: Spectra obtained with sequence *d* of Fig. 2 for $\tau_0 = 528\,\mu$s and $\tau' = 462$, 198, and 66 μs. In each case, the reversal of the time development during τ' leaves the net forward preparation time equivalent to that used for the corresponding spectrum at the left. The observed spectral distribution arises as the system evolves backwards in time from high-order to low-order coherences.

This demonstration of time reversal complements similar single-quantum approaches. For example, in the magic echo experiment, a pulse sequence applied to the system after the free induction signal has decayed can restore the signal to its initial intensity under ideal conditions. However, in the magic echo experiment there is no direct evidence that the time reversal is proceeding through multiple-spin events. By following the development of multiple-quantum coherence, we have shown here that time reversal can turn back the clock for coherent evolution involving large numbers of nuclear spins.

C. Dilute spin systems and clusters

An especially interesting potential application of multiple-quantum spectroscopy would be to characterize distributions of spins more directly than is possible with conventional single-quantum methods. Since multiple-quantum statistics are highly sensitive to the spatial arrangement of the nuclei, the time development of multiple-quantum coherence may vary significantly depending on whether the spins are distributed regularly or randomly, or grouped into dilute isolated clusters. In this section we consider how multiple-quantum excitation dynamics are affected by the different spatial distributions of spins encountered in individual systems. To facilitate these comparisons, we employ isotopic dilution to alter ^{1}H dipole–dipole interactions in a controlled fashion. The specific systems to be considered here are (1) a solid solution of HMB in perdeuterated HMB with a molar ratio of 1:10, (2) a sample of HMB randomly deuterated to a level of 80%–90%, and (3) a 1:20 solid solution of partially deuterated DMN in perdeuterated DMN. All the samples are polycrystalline, the mixtures having been obtained by evaporation of solvent.

1. Dilution effects—Hexamethylbenzene

Measured values of $N(\tau)$ for the two deuterated hexamethylbenzenes and for neat HMB are plotted in Fig. 11. It is evident that the same series of spectra is eventually obtained in each case, but that the preparation time required to realize a particular distribution depends strongly on the individual dipolar characteristics. Consequently, we can replace the independent variable τ by a scaled variable $a\tau$ to define a common time dependence for N. It is apparent from the data that $a = 1$ for neat HMB, $a = 1.65 \pm 0.10$ for the randomly deuterated material, and $a = 3.1 \pm 0.3$ for the 1:10 mixture.

Intramolecular dipolar couplings, presumably large, strongly influence multiple-quantum spectra at short preparation times. Since the dilution of HMB in a deuterated lattice does not affect these couplings, we might expect to see no changes in the initial development of coherence in the mixture. However, the straightforward scaling of the time dependence for $\tau \gtrsim 250\,\mu$s clearly indicates that the strongest intramolecular couplings have matured much earlier, apparently before 50–100 μs have elapsed. This is consistent with the crystal and molecular structure of HMB, which forces the longest intramolecular ^{1}H–^{1}H distances to be comparable to, and sometimes greater than the shortest intermolecular distances.[25] Therefore, except for couplings among the

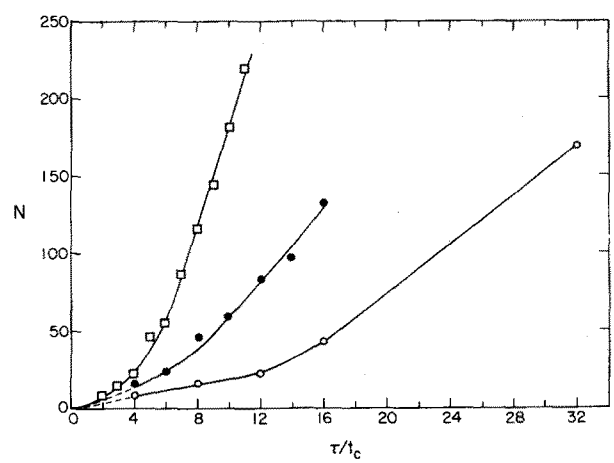

FIG. 11. N vs τ/t_c for neat hexamethylbenzene (squares), a 1:10 solid solution of HMB-h_{18} in HMB-d_{18} (open circles), and randomly deuterated HMB (shaded circles). The rates of increase of the effective size are slower in the two dilute systems.

three ^{1}H nuclei of a single methyl group, the distinction between intermolecular and intramolecular dipolar couplings is blurred in this system. Once interspin communication within one methyl group, and possibly with its two *ortho* neighbors, has been established at short τ, subsequent formation of coherence is likely to be dominated by intermolecular effects. These effects are attenuated, but not eliminated, by dilution. It is interesting to note here that the observed scaling factor of ~ 3 for $N(\tau)$ is close to the predicted scaling of the intermolecular dipolar linewidth by the square root of the concentration of protonated molecules in the dilute mixture.[32] This prediction follows from treating all distant molecules as point dipole sources, with each producing a local field averaged to one distinct value by the rapid sixfold molecular reorientation.

Random deuteration of HMB affects both intramolecular and intermolecular dipolar couplings to some extent. Analysis of this material by multiple-quantum spectroscopy enables us to distinguish it both from neat HMB and from the other dilute system with approximately the same total number of ^{1}H nuclei. The growth of $N(\tau)$ with τ for the randomly deuterated molecules is intermediate between the two extremes, a difference more striking than the subtler changes observable in the single-quantum ^{1}H spectra. We can account for the more rapid formation of spin correlations in the randomly deuterated sample, as compared to the 1:10 mixture, by noting that the distribution of ^{1}H nuclei is both higher and more uniform throughout the randomly deuterated material. More spins are in a position to communicate with each other at any given time.

2. Clustering effects—Dimethylnaphthalene

Clearly, if coherence in a solid is to be localized among a group of spins, there must exist a variation in dipolar couplings sharp enough to create isolated clusters on a specific experimental time scale. The basic requirement is for the couplings among proximate spins within a cluster to be sufficiently large as to preclude any communication with distant spins during the preparation period. In this situation the number of spins effectively interacting is limited, as in a liquid, and $N(\tau)$ should grow either very slowly or not at all once the strong couplings have matured. Where an isolated cluster does exist, multiple-quantum NMR can estimate the number of spins involved, thereby enhancing the more general information available from single-quantum line shape analysis.

The existence of local spin clusters can be discerned in the multiple-quantum spectra of dilute DMN, shown in Fig. 12 together with comparable spectra from neat DMN. The neat spin system is essentially unbounded, a state which is reflected in the spectra by a steady growth of the number of orders observed and of the parameter $N(\tau)$ used to characterize the distribution. In marked contrast, the spectra obtained from the 1:20 solid solution never extend beyond $n = 6$, and $N(\tau)$ increases only gradually from approximately 5 to 8 over the range $\tau = 66$ to $\tau = 462\ \mu$s. Since an N spin system will have coherences no greater than N, we can immediately establish $N = 6$ as a lower bound for the number of interacting spins in the dilute system. This is consistent with at least the

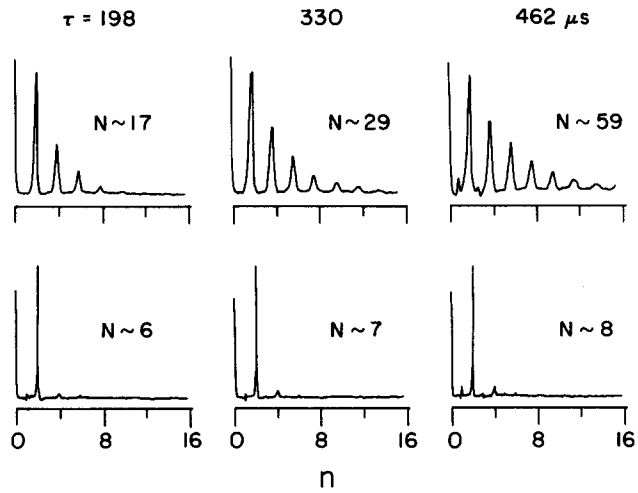

FIG. 12. 360 MHz ^{1}H multiple-quantum spectra of dimethylnaphthalene recorded with sequence (b) of Fig. 2. Top: Neat DMN, ring positions deuterated. Bottom: 1:20 solid solution in a perdeuterated host. The two sets of spectra clearly demonstrate the different multiple-quantum excitation pathways possible in bounded and unbounded spin distributions. Only low order coherence can develop among the six isolated spins in the diluted system; consequently the distribution of multiple-quantum intensity changes very little over the range of preparation times shown. By contrast, the effective size of the neat material increases continuously over the same range of times.

presence of the two neighboring protonated methyl groups in the large DMN molecule. Further dilution by large perdeuterated molecules creates the physical isolation necessary to excite the pairs of coupled methyl groups selectively. Small increases in $N(\tau)$ beyond 6 probably arise from the inevitable influence of long-range couplings as τ increases, and from the presence of a small percentage of 12-spin molecular dimers in the 1:20 mixture. The dilute spin system has a much more limited set of strong dipolar couplings than does the neat system, and hence the complicated coherences develop far more slowly in the dilute system.

V. SUMMARY

The development of multiple-quantum coherence in a system of coupled nuclei is a collective phenomenon, rooted in the concerted interaction of many spins. The dynamical evolution of such a system is determined largely by the complete network of spin–spin interactions, dominated initially by the largest couplings but ultimately affected by every spin present. The influence of weakly coupled, usually distant, spins grows with time, and with it so does the number of spins able to interact effectively. In this work, we have experimentally monitored the progressive development of dipole induced multiple-spin correlations by the detection of multiple-quantum spectra in systems of ^{1}H nuclei. We have noted that this continuous expansion of the spin system is an essential feature common to both the excitation of multiple-quantum coherence via a nonsecular Hamiltonian as well as to the decay of the free induction signal under normal dipolar evolution. The reversibility of multiple-quantum excitation has also been demonstrated explicitly here, thereby completing this link. Multiple-quantum events are thus re-

cognized as originating in rather fundamental processes in coupled systems.

The presence of an almost continuous range of dipolar couplings in a typical solid often makes it unrealistic to draw artificial boundaries delineating molecules or functional groups. Consequently, multiple-quantum coherence can extend over large numbers of spins, and involve transitions of very high order. Here, we have taken a statistical approach to the development and distribution of coherence in these large systems, based upon the assumption of equal coherence magnitudes over long periods of excitation. In this view, the intensity distribution of a multiple-quantum spectrum is described roughly by a Gaussian, which is characterized by a variance proportional to the instantaneous spin size. The effective size, $N(\tau)$, is best regarded as a parameter reflecting both the expansion of the coupling network with time and the growing in and maturing of lower-order coherences. A random walk, or diffusive, picture is then used to model the apparently monotonic increase of $N(\tau)$ under the influence of the coupling Hamiltonian.

Finally, we have shown that where isolated clusters of spins exist in a solid, multiple-quantum spectroscopy can be used as a rudimentary "spin counting" tool. However, isolation is always a relative concept in a dipolar solid, and must be defined operationally with reference to a certain experimental time scale. The results presented here have demonstrated that spin counting can be accomplished successfully, provided that there exists a sharp disparity between intra- and intercluster dipole couplings. We expect these methods to be applied fruitfully to a variety of systems in chemistry and physics, especially to molecules isolated in matrices or adsorbed on surfaces.[33]

ACKNOWLEDGMENTS

We thank R. Tycko and D. P. Weitekamp for several useful discussions throughout the course of this work. The crystal of squaric acid was kindly provided by M. Mehring. One of us, ANG, was supported by the advanced research program of the Naval Research Laboratory. This work was supported by the U. S. Department of Energy through the Director's Program Development Funds of the Lawrence Berkeley Laboratory under Contract Number DE-AC03-76SF00098.

[1]G. Bodenhausen, Prog. NMR Spectrosc. **14**, 137 (1981).
[2]D. P. Weitekamp, Adv. Magn. Reson. **11**, 111 (1983).
[3]U. Fano, Rev. Mod. Phys. **29**, 74 (1957).
[4](a) S. Vega and A. Pines, J. Chem. Phys. **66**, 5624 (1977); (b) S. Vega, *ibid.* **68**, 5518 (1978); (c) A. Wokaun and R. R. Ernst, *ibid.* **67**, 1752 (1977).
[5]G. Drobny, A. Pines, S. Sinton, D. P. Weitekamp, and D. Wemmer, Faraday Symp. Chem. Soc. **13**, 49 (1979).
[6](a) O. W. Sørensen, G. W. Eich, M. H. Levitt, G. Bodenhausen, and R. R. Ernst, Prog. NMR Spectrosc. **16**, 163 (1983); (b) K. J. Packer and K. M. Wright, Mol. Phys. **50**, 797 (1983).
[7](a) W. S. Warren, D. P. Weitekamp, and A. Pines, J. Chem. Phys. **73**, 2084 (1980); (b) G. Drobny, A. Pines, S. Sinton, W. S. Warren, and D. P. Weitekamp, Philos. Trans. R. Soc. London Ser. A **299**, 585 (1981); (c) W. S. Warren and A. Pines, J. Chem. Phys. **74**, 2808 (1981); (d) S. Sinton, D. B. Zax, J. B. Murdoch, and A. Pines, Mol. Phys. **53**, 333 (1984).
[8](a) A. Bax, R. Freeman, and S. P. Kempsell, J. Magn. Reson. **41**, 349 (1980); (b) J. Am. Chem. Soc. **102**, 4851 (1980); (c) A. Bax, R. Freeman, and T. A. Frenkiel, *ibid.* **103**, 2102 (1981); (d) U. Piantini, O. W. Sørensen, and R. R. Ernst, J. Am. Chem. Soc. **104**, 6800 (1982); (e) M. H. Levitt and R. R. Ernst, Chem. Phys. Lett. **100**, 119 (1983); (f) L. Braunschweiler, G. Bodenhausen, and R. R. Ernst, Mol. Phys. **48**, 535 (1983).
[9](a) D. P. Weitekamp, J. R. Garbow, J. B. Murdoch, and A. Pines, J. Am. Chem. Soc. **103**, 3578 (1981); (b) J. R. Garbow, D. P. Weitekamp, and A. Pines, J. Chem. Phys. **79**, 5301 (1983).
[10](a) L. Mueller, J. Am. Chem. Soc. **101**, 4481 (1979); (b) Y. S. Yen and D. P. Weitekamp, J. Magn. Reson. **47**, 476 (1982); (c) A. Bax, R. H. Griffey, and B. L. Hawkins, *ibid.* **55**, 301 (1983).
[11]Y. S. Yen and A. Pines, J. Chem. Phys. **78**, 3579 (1983).
[12](a) R. H. Schneider and H. Schmiedel, Phys. Lett. A **30**, 298 (1969); (b) W. K. Rhim, A. Pines, and J. S. Waugh, Phys. Rev. Lett. **25**, 218 (1970); (c) W. K. Rhim, A. Pines, and J. S. Waugh, Phys. Rev. B **3**, 684 (1971); (d) A. Pines, W. K. Rhim, and J. S. Waugh, J. Magn. Reson. **6**, 457 (1972).
[13]I. J. Lowe and R. E. Norberg, Phys. Rev. **107**, 46 (1957).
[14]W. P. Aue, E. Bartholdi, and R. R. Ernst, J. Chem. Phys. **64**, 2229 (1976).
[15]A. N. Garroway, J. Baum, M. G. Munowitz, and A. Pines, J. Magn. Reson. **60**, 337 (1984).
[16]A. Pines, D. Wemmer, J. Tang, and S. Sinton, Bull. Am. Phys. Soc. **23**, 21 (1978).
[17]G. Bodenhausen, R. L. Vold, and R. R. Vold, J. Magn. Reson. **37**, 93 (1980).
[18]E. O. Stejskal and J. Schaefer, J. Magn. Reson. **18**, 560 (1975).
[19]G. Drobny, Ph.D. thesis, University of Calif., Berkeley, 1982 (published as Lawrence Berkeley Laboratory Report LBL-15254).
[20]J. R. Garbow, Ph.D. thesis, University of Calif., Berkeley, 1983 (published as Lawrence Berkeley Laboratory Report LBL-16119).
[21]W. K. Rhim, D. D. Elleman, L. B. Schreiber, and R. W. Vaughan, J. Chem. Phys. **60**, 4595 (1974).
[22]U. Haubenreisser and B. Schnabel, J. Magn. Reson. **35**, 175 (1979).
[23]A. Garroway, J. Magn. Reson. **63**, 504 (1985).
[24]W. Nowacki, Helv. Chim. Acta **28**, 1233 (1945).
[25]See R. W. C. Wyckoff, *Crystal Structures* (Interscience New York, 1966), Vol. 6, Part 1, p. 386.
[26](a)E. R. Andrew, J. Chem. Phys. **18**, 607 (1950); (b) D. E. Wemmer, Ph.D. thesis, University of California, Berkeley, 1978, pp. 38–43 (published as Lawrence Berkeley Laboratory Report LBL-16119).
[27](a) D. Semmingsen and J. Feder, Solid State Commun. **15**, 1369 (1974); (b) E. J. Samuelsen and D. Semmingsen, *ibid.* **17**, 217 (1975).
[28]D. Bright, I. E. Maxwell, and J. de Boer, J. Chem. Soc. Perkin Trans. 2 **1973**, 2101.
[29](a) R. A. Hoffman, Adv. Magn. Reson. **4**, 87 (1970); (b) A. Wokaun and R. R. Ernst, Mol. Phys. **36**, 317 (1978).
[30]J. B. Murdoch, W. S. Warren, D. P. Weitekamp, and A. Pines, J. Magn. Reson. **60**, 205 (1984).
[31]N. Bloembergen, Physica **15**, 386 (1949).
[32]C. Kittel and E. Abrahams, Phys. Rev. **90**, 238 (1953).
[33]P. K. Wang, C. P. Slichter, and J. H. Sinfelt, Phys. Rev. Lett. **53**, 82 (1984).